ATLAS NOTE

ATLAS-CONF-2011-094

July 14, 2011

A Search for a light charged Higgs boson decaying to $c\bar{s}$ in pp collisions at $\sqrt{s}$ = 7 TeV with the ATLAS detector

The ATLAS Collaboration

Abstract

We present the search results for a light charged Higgs boson produced in top quark decays and decaying into two jets in pp collisions at $\sqrt{s}$ = 7 TeV with the ATLAS detector. The analysis uses the data sample collected during 2010, corresponding to an integrated luminosity of 35 pb^{-1}. The search is based on the semi-leptonic decay channel of $t\bar{t}$ candidates and analyzes the invariant mass distribution of two jets in the final state. The data are found to be in good agreement with the expectation from the Standard Model background processes and 95% upper limits are set on the decay branching ratio of top quarks to charged Higgs bosons that decay into $c\bar{s}/\bar{c}s$.

1 Introduction

In the Standard Model (SM) electroweak symmetry breaking (EWSB) [1, 2, 3] occurs through a single complex scalar doublet field. This results in a single observable Higgs boson, which has not yet been discovered. Consequently, the mechanism of EWSB remains in question. Beyond the SM, many models [4] have been proposed to extend the Higgs sector to explain EWSB. A simple extension is the two Higgs-doublet model (2HDM) [4, 5]. In the 2HDM, there are five physical states. Two of them are charged (H^+ and H^-) and three are neutral. The discovery of charged Higgs bosons would be a definite signal for new physics beyond the SM.

The Minimal Supersymmetric Standard Model (MSSM) [4, 6] is an example of a 2HDM. At tree level, the MSSM Higgs sector is determined by two independent parameters only, usually chosen for H^+ studies to be the mass m_{H^+} and the ratio of the two Higgs doublet vacuum expectation values, $\tan\beta$. In the MSSM, a light H^+ decays primarily to $c\bar{s}$[1] , $b\bar{b}W^+$ and $\tau^+\nu$, with the respective branching ratios depending on $\tan\beta$ and m_{H^+}. For $\tan\beta < 1$, $c\bar{s}$ is an important decay mode with $\mathcal{B}(H^+ \to c\bar{s})$ near 40% for $m_{H^+} \simeq 130$ GeV. For $\tan\beta > 3$, $H^+ \to \tau^+\nu$ dominates (90%).

The LEP experiments placed lower limits on m_{H^+} in any type-II 2HDM [7] of between 79 and 90 GeV [8] depending on the assumed decay branching ratios for the charged Higgs boson. At the Tevatron, searches for MSSM Higgs bosons in $p\bar{p}$ collisions have been extended to larger values of m_{H^+}. No evidence has been found for a charged Higgs boson and upper limits were set on the branching ratio $\mathcal{B}(t \to H^+b)$ of a light H^+ ($m_{H^+} < m_{top}$) [9, 10].

In this Note, a search for charged Higgs bosons in semi-leptonic $t\bar{t}$ events is presented, where one of the top quarks decays as $t \to H^+b$ with the charged Higgs boson subsequently decaying to two light jets ($c\bar{s}$ or $u\bar{d}$). The other top quark decays as $\bar{t} \to W^-\bar{b}$ and the W boson decays into an electron or a muon and a neutrino. The signal has the same characteristics as semi-leptonic $t\bar{t}$, with the exception of the mass of the two jets from the H^+, which will peak at m_{H^+}, rather than m_W. The presence of a signal would also result in a reduced number of events in the lepton plus jets final state because of the additional all hadronic decay mode $t\bar{t} \to H^+bH^-\bar{b}$. Therefore a search is performed by comparing the dijet mass spectrum in the data with the expection from SM top decays and the expectation when the top quark has a non-zero branching ratio to decay to H^+b, which gives a second peak around m_{H^+}. The theoretical calculation of the $t\bar{t}$ production cross section is used as a prior constraint and as such the search is sensitive to both the overall number of events observed and the shape of the dijet mass spectrum.

2 Monte Carlo and Data Samples

The largest background to the charged Higgs boson signal comes from the production of SM decays of $t\bar{t}$. The rest of the SM backgrounds (referred as non-$t\bar{t}$ backgrounds) are single top, W/Z+jets, diboson and QCD multijet events. Top pair and single top events have been generated using the MC@NLO 3.41 [11] Monte Carlo (MC) generator coupled to HERWIG and JIMMY [12] to provide the parton shower and hadronization models using the AUET1-CTEQ66 [13] tune. W/Z+jet and diboson events are generated using the leading order (LO) ALPGEN [16] generator interfaced to HERWIG and JIMMY using the AUET1-CTEQ6L1 tune. The W/Z+jet samples include dedicated samples for $W/Z + b\bar{b}$ production. Signal samples of $t\bar{t} \to H^+bW^-\bar{b}$ are generated using PYTHIA [17] and the AMBT1 [14] tune. In this MC sample the width of the charged Higgs boson is taken to be zero. This is a good approximation for a charged Higgs boson with a width which is small compared with the experimental resolution. All the generated events are passed through a full simulation of the ATLAS detector [18] and are then reconstructed in the same way as the data. The MC samples are normalized using the appropriate theoretical cross sections [19, 20, 21, 22, 23, 24]. Corrections to the simulation for lepton reconstruction, trigger efficiencies

[1] In this Note, charge conjugation is assumed throughout.

and lepton momentum scale / resolution are derived from the data and applied to the MC. Backgrounds from QCD multijet events are estimated from the data itself.

The data used in the analysis were recorded by the ATLAS detector between June and November 2010 during the proton-proton collisions at $\sqrt{s} = 7$ TeV. The ATLAS detector [25] consists of an inner tracking system immersed in a 2 T magnetic field provided by a thin solenoid, electromagnetic and hadronic calorimeters, and a muon spectrometer (MS). The inner detector tracking system (ID) is made up of a silicon pixel detector closest to the beam line, followed by a silicon microstrip detector and a transition radiation tracker. The electromagnetic (EM) calorimeters are high granularity liquid-argon (LAr) sampling calorimeters. The hadronic calorimetry uses two different detector technologies. The active material is either scintillating tiles or LAr and the absorber material is steel, copper or tungsten. The MS consists of three large superconducting toroids each with eight coils and a system of both precision and fast trigger chambers. Events are required to pass a high-p_T electron or muon trigger, and to have been recorded when all detector systems critical to muon, electron and jet identification were flagged as good for physics analysis. The triggers used in the different data taking periods had lepton transverse momentum thresholds varying from 10 to 15 GeV. The resulting dataset corresponds to an integrated luminosity of 35 pb^{-1} [15].

3 Object and Event Selection

Muons are required to be identified in both the ID and MS systems and a combined fit is performed for all the hits to obtain the momentum of the muon [26]. Muons are required to pass isolation criteria to reject those from heavy flavor decays and hadrons misidentified as muons. The sum of the transverse momenta of ID tracks found within a cone of $\Delta R = \sqrt{(\Delta\phi)^2 + (\Delta\eta)^2} = 0.3$ of the muon is required to be less than 4 GeV [2]. The transverse energy measured in the calorimeters in a cone of $\Delta R = 0.3$, excluding the energy associated with the muon, is required to be less than 4 GeV.

Electrons are reconstructed in the calorimeter, starting from a seed cluster in the second layer of the EM calorimeter. The cluster is matched to a track found in the ID and a set of selection criteria are applied to reject electron candidates originating from jets [27]. Electrons are required to be isolated by ensuring that the transverse energy measured in the calorimeters in a cone of $\Delta R = 0.2$, excluding the electron itself, is less than 4 GeV.

Jets are reconstructed from clusters of calorimeter cells using the anti-k_t algorithm [28] with a radius parameter $R = 0.4$. Jets are corrected back to particle level using calibrations that are derived from MC and validated with both test-beam [29] and collision-data studies [30]. Events are rejected if they contain a high-p_T jet that fails quality criteria which reject detector noise and non-collision backgrounds. Jets from b-quark decays are identified using a secondary vertex algorithm [34], which attempts to reconstruct the secondary vertex formed by the decay products of the b-hadron. Jets passing the secondary vertex algorithm selection are referred to as b-tagged jets. The selection on the discriminating variable of the algorithm achieves a 50% efficiency to select b-jets in $t\bar{t}$ events, with a probability to incorrectly identify light jets of less than 0.4%.

The missing transverse energy, $E_{\mathrm{T}}^{\mathrm{miss}}$, is constructed from the vector sum of calorimeter energy deposits, resolved into the transverse plane. Cells not associated to muons, electrons with transverse momentum above 10 GeV, photons, taus and jets are included at the electromagnetic energy scale. The electrons, muons and jets used in the $E_{\mathrm{T}}^{\mathrm{miss}}$ calculation are used consistently with the definitions stated above.

[2] ATLAS uses a right-handed coordinate system with its origin at the nominal interaction point in the center of the detector. Cylindrical coordinates (r, ϕ) are used in the transverse plane, ϕ being the azimuthal angle around the beam axis. The pseudo-rapidity is defined in terms of the polar angle θ as $\eta = ln\tan(\theta/2)$.

Events must pass a set of requirements designed to select semi-leptonic $t\bar{t}$ events [31], which have one energetic lepton, multiple jets and the signature of a neutrino. Exactly one lepton (electron or muon) with a high transverse momentum ($p_{\mathrm{T}} > 20$ GeV) is required. The selected lepton is required to match a trigger object that caused the event to be recorded. To suppress backgrounds from QCD multijet events, the missing transverse energy is required to be $E_{\mathrm{T}}^{\mathrm{miss}} > 20(35)$ GeV in the muon (electron) channel. Further reduction of the multijet background is achieved by requiring the transverse invariant mass (M_T) of the lepton and $E_{\mathrm{T}}^{\mathrm{miss}}$ to satisfy $M_T > 25$ GeV in the electron channel and $E_{\mathrm{T}}^{\mathrm{miss}} + M_T > 60$ GeV in the muon channel. The selections are more stringent in the electron channel because of the larger multijet background. The background from W + jet events is reduced by requiring at least four jets with $p_{\mathrm{T}} > 25$ GeV and $|\eta| < 2.5$. At least one jet must be identified as originating from a b-decay using the secondary vertex algorithm.

4 Kinematic Fit

In lepton plus four jets events, the two jets originating from decays of H^+ need to be identified in order to reconstruct the mass of H^+ candidates. A kinematic fitter [9] is used to identify and reconstruct the mass of dijets from W/H^+ candidates, by fully reconstructing the $t\bar{t}$ system. In the kinematic fitter, the lepton, the $E_{\mathrm{T}}^{\mathrm{miss}}$ (from the neutrino), and four jets are assigned to the decay partons from the $t\bar{t}$ system. The world average of the W boson mass [35] is used to calculate the longitudinal momentum of the neutrino. This results in two possible solutions for this momentum. The fitter also constrains the two b-jet and W/H^+ boson systems (blv, bjj) to have the measured top quark mass [36] within $\sigma_{top} = 1.5$ GeV. When assigning jets in the fitter, b-tagged jets are assumed to originate from the b-quarks. The best combination is found by minimizing a χ^2 for each assignment of jets to quarks, where up-to the five leading jets are considered as possible top decay products. The different jet to quark assignments and the two neutrino solutions give 12 possible combinations for a four-jet event, where one jet has been identified as originating from a b-quark. For five jet events, the two leading jets are always assumed to be top decay products to reduce the combinatorics in the fit procedure. The combination with the smallest χ^2 value is selected as the best assignment. The function minimised in the fit is:

$$\begin{aligned}\chi^2 = & \sum_{i=l,4jets} \frac{(p_T^{i,fit} - p_T^{i,meas})^2}{\sigma_i^2} \\ & + \sum_{j=x,y} \frac{(p_j^{UE,fit} - p_j^{UE,meas})^2}{\sigma_{UE}^2} \\ & + \sum_{k=bjj,blv} \frac{(M_k - M_{top})^2}{\sigma_{top}^2}.\end{aligned} \tag{1}$$

In the fit, the measured energies of the leptons and jets ($p_T^{i,meas}$) are allowed to vary within their measured resolutions (σ_i). The unclustered energy (p^{UE}) is the sum of measured transverse energies not associated with the leading four jets and lepton. This term encapsulates all the measurements that contribute to the transverse missing energy that are not included in the other two terms in the χ^2. Since the UE term is dominated by additional jets, the resolution of the UE is extrapolated from the jet resolution. The fit results in a significant reduction in the width of the dijet mass distribution (m_{jj}) predicted by the MC as shown in Fig. 1. This figure also shows an good discrimination between the mass peaks of the W boson from the SM decays of $t\bar{t}$ and the H^+ boson. The χ^2 distribution agrees well between the data and the expectation from the simulation (Fig. 2). Events are required to have a fit $\chi^2 < 20$ to remove poorly reconstructed $t\bar{t}$ events. This selection has an efficiency of 82% for $t\bar{t}$ events.

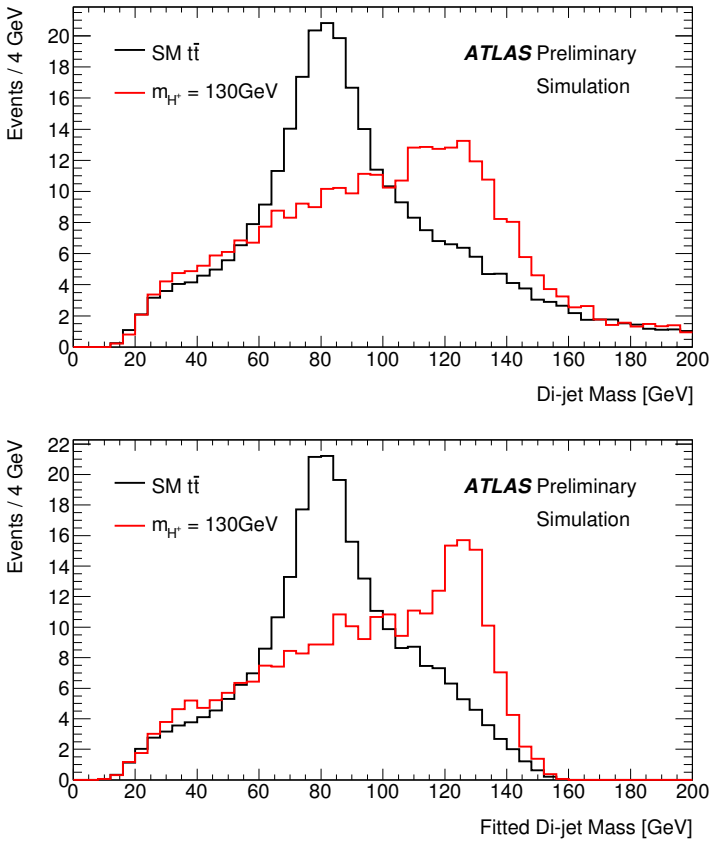

Figure 1: Comparison of the dijet mass distribution before (top) and after (bottom) the kinematic fit and $\chi^2 < 20$ cut. The distribution is shown for MC simulations of SM $t\bar{t}$ decays and the signal ($t\bar{t} \to H^+bW^-\bar{b}$).

5 Results and Systematic Uncertainties

The number of observed events in the data after the selection requirements agrees well with the expectation from the SM background processes (Table 1). The size of the QCD multijet background has been modelled here by data driven methods [31]. This multijet background includes contributions from leptons from heavy-quark decays and also from hadrons that are misidentified as leptons. In the muon+jets channel, where leptons from heavy-quark decays dominate, a 'matrix method' estimate is used and in the electron+jets channel a binned likelihood template fit based on the $E_{\mathrm{T}}^{\mathrm{miss}}$ distribution is used. The number of expected background and signal events in Table 1 depends on various effects that introduce the following systematic uncertainties into the expectations: integrated luminosity (3.4%)[15], trigger efficiency (0.2/0.8% for electron / muon), lepton reconstruction (3.9/0.4% for electron / muon), jet energy scale, jet energy resolution, and b-jet identification efficiency. The later three uncertainties depend on the p_{T} and η of the jets. An additional uncertainty is placed on the b-jet energy scale (2.5%). In addition, uncertainties on the modeling of the $t\bar{t}$ background are estimated by using a second MC generator (Powheg [37]) and by comparing the effect of using Pythia and Herwig to perform the parton showering and hadronization. Uncertainties on initial and final state radiation (ISR / FSR) are assessed by using AcerMC [38] interfaced to Pythia and examining the effects of changing the ISR / FSR parameters in a range consistent with experimental data [26]. The uncertainty due to the modelling of additional

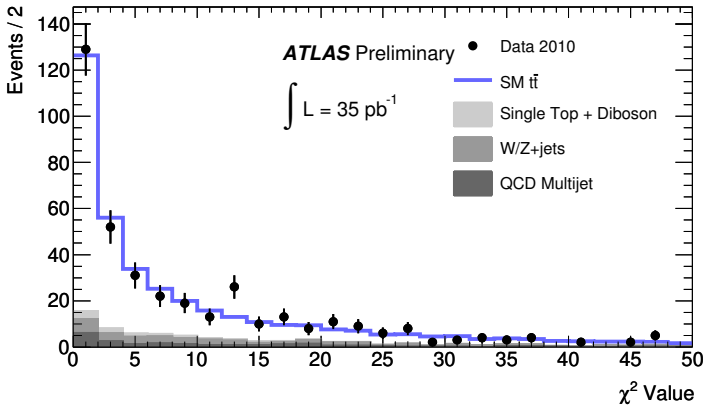

Figure 2: Comparison of the fit χ^2 distribution of the data with the expectation from the background estimates for the combined electron and muon channels. The MC is normalised to the expectation for the SM ($\mathcal{B}(t \to H^+ b) = 0$).

pp interactions in the MC is 5%. The theoretical uncertainty on the total $t\bar{t}$ production cross section is +7.0%, −9.6%. An additional uncertainty on the cross section from the uncertainty on the top quark mass is also included (7%). The uncertainty on the top mass from the latest Tevatron dilepton measurements [32, 33] was used to avoid possible bias from a $H^+ \to c\bar{s}$ signal in the lepton+jets channel. Most of these uncertainties affect only the overall acceptance for the signal and background and this can be seen in Table 2, however the jet energy calibration, b-jet identification, $t\bar{t}$ background modeling and ISR / FSR uncertainties modify the shape of the dijet mass distribution and so are parameterized in m_{jj}. The rate of $W+ \geq 4$ jet events predicted by the MC has a large theoretical uncertainty and so this uncertainty is estimated using the data. Events are selected using the same criteria as described above, but omitting the requirement of at least one jet being identified as originating from a b-quark. The rate of W+jets and $t\bar{t}$ events is then extracted by fitting the lepton η distribution predicted by the MC samples to the observed data. The lepton η distribution is used because the signal and SM $t\bar{t}$ background events have the same shape, whereas the W+jets events have a different (broader) shape. This procedure yields an uncertainty of 26% on the W+jets normalization. An additional uncertainty on the W+jets background of 22% is ascribed to account for the uncertainty in incorrectly identifying light jets as b-tagged jets. The QCD multijet background model is assigned a 30/50% uncertainty in the muon and electron channels respectively.

The data are found to agree well with the distribution of the dijet mass expected from the background processes (Fig. 3) and upper limits are extracted on the branching ratio $\mathcal{B}(t \to H^+ b)$ as a function of the charged Higgs boson mass. The upper limits assume the charged Higgs boson decays 100% of the time into $c\bar{s}$. The following likelihood function is used to describe the expected number of signal and background events as a function of the branching ratio:

$$\mathcal{L}(\mathcal{B}, \alpha) = \prod_i \frac{\nu_i^{n_i} e^{-\nu_i}}{n_i!} \prod_j \frac{1}{\sqrt{2\pi}} e^{-\frac{\alpha_j^2}{2}}, \tag{2}$$

where n_i is the number of events observed in bin i of the dijet mass distribution and j labels the systematic

Channel	Muon	Electron
Data	193	130
SM $t\bar{t} \to W^+bW^-\bar{b}$	156^{+24}_{-29}	106^{+16}_{-20}
W/Z + jets	17 ± 6	9 ± 3
Single top	7 ± 1	5 ± 1
Diboson	0.30 ± 0.02	0.20 ± 0.02
QCD multijet	11 ± 4	6 ± 3
Total Expected (SM)	191^{+26}_{-30}	127^{+17}_{-21}
$\mathcal{B}(t \to H^+b) = 10\%$:		
$t\bar{t} \to H^+bW^-\bar{b}$	20^{+3}_{-4}	14^{+2}_{-2}
$t\bar{t} \to W^+bW^-\bar{b}$	127^{+19}_{-23}	86^{+13}_{-16}
Total Expected ($\mathcal{B} = 10\%$)	181^{+21}_{-25}	120^{+14}_{-17}

Table 1: The expected number of events from the SM background processes is compared with the observed number of events in the data after all the selection requirements. The expected number of events in the case of a signal with $m_{H^+} = 110$ GeV and $\mathcal{B}(t \to H^+b) = 10\%$ is also shown. The uncertainties shown are the sum of the statistical and systematic uncertainties.

Systematic Source	
Jet energy scale	$+11, -13\%$ (SM $t\bar{t}$)
	$+9, -12\%$ (signal)
b-Jet energy scale	$\pm 0.5\%$
Jet energy resolution	$\pm 1\%$
b-tagging efficiency	$+4, -9\%$
MC generator	$\pm 4\%$
Parton shower	$\pm 3\%$
ISR/FSR	$\pm 1\%$
Additional Interactions	$\pm 4\%$
Luminosity	$\pm 3.4\%$
Electron reconstruction	$\pm 1.6\%$
Muon reconstruction	$\pm 0.2\%$
Electron trigger	$\pm 0.2\%$
Muon trigger	$\pm 0.5\%$
$t\bar{t}$ cross section	$+7, -9\%$
t quark mass	$\pm 7\%$

Table 2: Effect of the systematic uncertainties on the expected number of $t\bar{t}$ background and signal ($m_{H^+} = 110$ GeV) events. Where only one uncertainty is given, the effect is the same for both the signal and $t\bar{t}$ background.

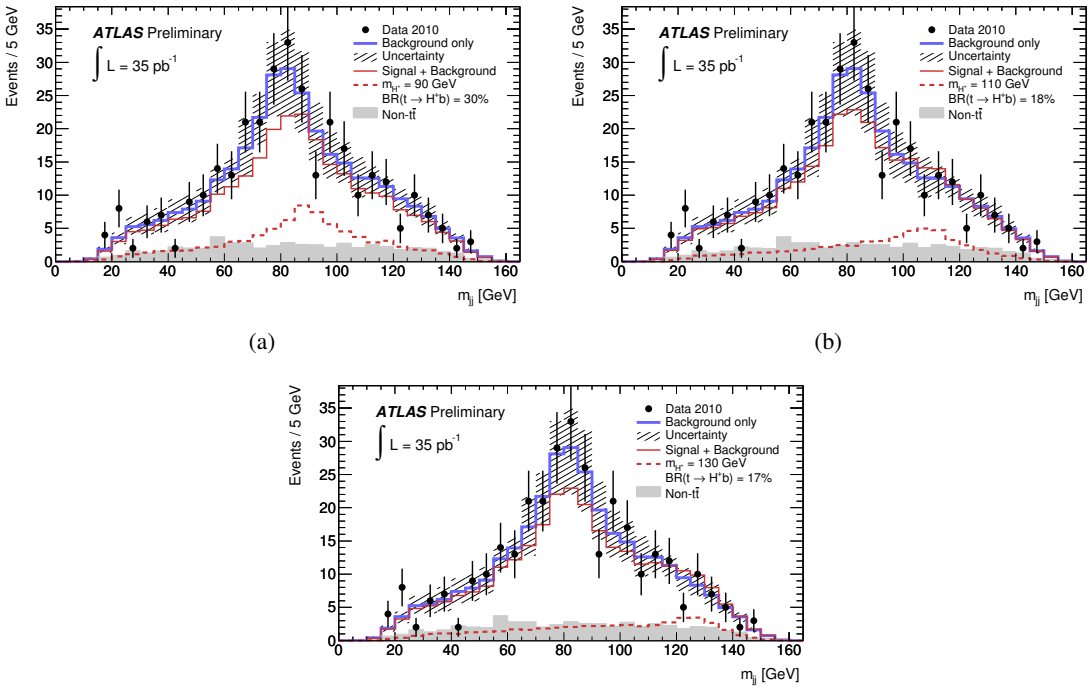

Figure 3: The dijet mass distribution of the data is compared with the expectation from the SM ($\mathcal{B} = 0$) and with (a) the expectation with $\mathcal{B} = 0.30$ ($m_{H^+} = 90$ GeV), (b) the expectation with $\mathcal{B} = 0.18$ ($m_{H^+} = 110$ GeV) and (c) the expectation with $\mathcal{B} = 0.17$ ($m_{H^+} = 130$ GeV). The error bars represent the statistical uncertainty from the data. The uncertainty shown on the background estimate is the combination in quadrature of the fractional uncertainties of the $\pm 1\sigma$ systematic uncertainties. The size of these uncertainties can be constrained by the data in the likelihood fit. The fractional uncertainty on the signal-plus-background model is comparable to the background-only model.

source. The number of expected events, ν_i in each bin, is given by

$$\begin{aligned}\nu_i = {} & 2\mathcal{B}(1-\mathcal{B})\sigma_{t\bar{t}} L \varepsilon_i^{H^+} \prod_j \rho_{ji}^{H^+}(\alpha_j) \\ & + (1-\mathcal{B})^2 \sigma_{t\bar{t}} L \varepsilon_i^{W} \prod_j \rho_{ji}^{W}(\alpha_j) + n_i^b \prod_j \rho_{ji}^{b}(\alpha_j)\end{aligned} \tag{3}$$

where n_i^b is the expected number of non-$t\bar{t}$ background events, $\sigma_{t\bar{t}}$ is the cross-section for top pair production, L is the integrated luminosity, $\mathcal{B}$ is the branching ratio of $t \to H^+ b$ and $\varepsilon_i^{H^+}$, ε_i^W are the efficiencies to select signal ($t\bar{t} \to H^+ b W^- \bar{b}$) and SM $t\bar{t}$ ($t\bar{t} \to W^+ b W^- \bar{b}$) events respectively. The value for the $t\bar{t}$ cross section (165 pb) is calculated at approximate NNLO with the `Hathor` program [19]. The decay mode $t\bar{t} \to H^+ b H^- \bar{b}$ does not contribute to the expectation because this mode does not produce an isolated lepton and hence has a negligible efficiency to pass the selection requirements. The ρ_{ji} and α_j parameters contain the effects of the systematic uncertainties and are defined such that $\rho_{ji}(\alpha_j = \pm 1)$ represents the $\pm 1\sigma$ fractional change in the dijet mass spectrum of systematic j. Each systematic uncertainty is considered correlated between signal and background and un-correlated from the other systematic uncertainties. The α_j variables are parameters in the fit that are constrained via the Gaussian terms in Equation 2. Since the final data sample contains a significant number of events, the effect of the systematic uncertainties

Higgs Mass	Expected limit	Observed limit
90 GeV	0.30	0.25
110 GeV	0.18	0.15
130 GeV	0.17	0.14

Table 3: Expected and observed 95% CL limits on the branching ratio of top to a charged Higgs boson and a b-quark. The limits shown are calculated using the CL_s limit setting procedure.

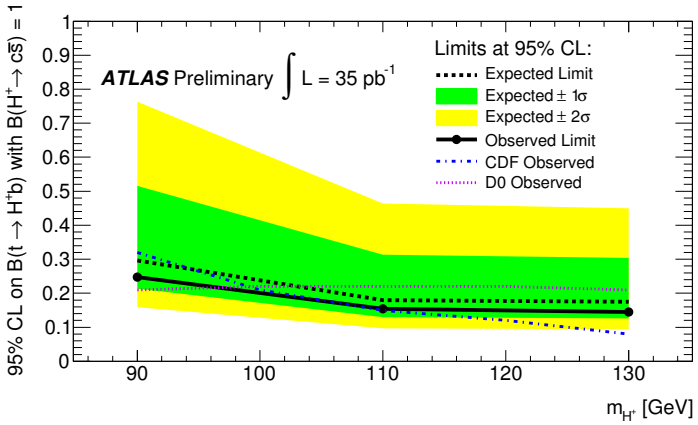

Figure 4: The extracted 95% C.L. upper limits on $\mathcal{B}(t \to H^+b)$ from the ATLAS data are compared with the expected results and results from the Tevatron. The results assume $\mathcal{B}(H^+ \to c\bar{s} = 100\%)$. The ATLAS limits shown are calculated using the CL_s limit setting procedure.

on m_{jj} can be constrained when the likelihood fit is performed. Note that the total number of expected events decreases with increasing signal $\mathcal{B}$. The limits are extracted with a fully-frequentist technique using a test statistic based on the profile likelihood ratio [39] by finding the $\mathcal{B}$ for which the confidence level in the signal hypothesis (CL_s [40]) reaches 0.05, where CL_s is defined as:

$$CL_s = \frac{CL_{s+b}}{CL_b}. \tag{4}$$

Limits constructed from CL_s over-cover by construction, however the technique avoids excluding very small signal rates due to downward fluctuations in the background. The consistency of the data with the background model can be determined by comparing the value of the test statistic in the data with the expectation from background-only toy experiments. The corresponding p-value varies from 0.67 to 0.71 as a function of m_{H^+}, indicating that there is no significant deviation from the background hypothesis. The expected and observed limits are calculated using the asymptotic formulae [39] and are shown in Table 3. The limits are also shown in Fig. 4 where the extracted limits are compared with the previous limits from the Tevatron [9, 10]. The sensitivity of the analysis presented in this Note is comparable to the limits obtained at the Tevatron, where datasets with more than twenty-five times the integrated luminosity were used.

6 Conclusions

A search for charged Higgs bosons produced via the decay of top quarks has been presented. The dijet mass distribution is in good agreement with the expectation from the SM and limits are set on the

branching ratio $\mathcal{B}(t \to H^+ b)$, assuming $\mathcal{B}(H^+ \to c\bar{s}) = 100\%$. The observed limits are within one standard deviation of the expected limits and range from $\mathcal{B} = 0.25$ to 0.14 for $m_{H^+} = 90$ to 130 GeV. These are the first limits on charged Higgs bosons in this channel from the LHC. This result can be used to set limits for an anomalous scalar charged boson decaying to dijets in top quark decays, as no model-specific parameters are used in this analysis.

References

[1] F. Englert and R. Brout, Phys. Rev. Lett. **13**, 321 (1964).

[2] P. W. Higgs, Phys. Lett. **12** 132(1964).

[3] G. Guralnik et al, Phys. Rev. Lett. **13** 585 (1964).

[4] J.F. Gunion *et al.*, "The Higgs Hunter's Guide", Addison-Wesley (1990).

[5] Y. Grossman, Nucl. Phys. B **426**, 355 (1994).

[6] S. Dimopoulos, H. Georgi Nucl. Phys. B **193**, 150 (1981).

[7] V. Barger, J. L. Hewett, and R. J. N. Phillips, Phys. Rev. D **41**, 3421–3441 (1990).

[8] ALEPH Collaboration, Phys. Lett. B **543**, 1 (2002); DELPHI Collaboration, Phys. Lett. B **525**, 17 (2002); L3 Collaboration, Phys. Lett. B **575**, 208 (2003); OPAL Collaboration, Eur. Phys. J. C7, 407 (1999); LEP Working Group for Higgs Boson Searches, arXiv:0107031 [hep-ex].

[9] T. Aaltonen *et al.* (CDF Collaboration), Phys. Rev. Lett. **103**, 101803 (2009).

[10] V. M. Abazov *et al.* (D0 Collaboration), Phys. Lett. B **682**, 278 (2009).

[11] S. Frixione and B.R. Webber, JHEP **0206** (2002) 029; S. Frixione, P. Nason and B.R. Webber, JHEP **0308** (2003) 007.

[12] G. Corcella *et al.*, JHEP **0101** (2001) 010.

[13] ATLAS Collaboration, ATLAS-PHYS-PUB-2010-014 (2010).

[14] ATLAS Collaboration, ATLAS-CONF-2010-031 (2010).

[15] ATLAS Collaboration, ATLAS-CONF-2011-011 (2011).

[16] M. L. Mangano *et al.*, JHEP **0307**, 001 (2003).

[17] T. Sjostrand, S. Mrenna and P. Z. Skands, JHEP **0605**, 026 (2006).

[18] ATLAS Collaboration, Eur. Phys. J. C **70**, 823 (2010).

[19] M. Aliev et al., Comput. Phys. Commun. **182**, 1034 (2011).

[20] S. Moch, P. Uwer, Nucl. Phys. Proc. Suppl.**183** 7580 (2008).

[21] U. Langenfeld, S. Moch, and P. Uwer, arXiv:0907.2527 [hep-ph].

[22] C. Anastasiou et al., Phys. Rev. D **69**, 094008 (2004).

[23] S. Frixione et al., JHEP 07 (2008) 029.

[24] J.M.Campbell, R.K.Ellis, Phys. Rev. D**60** 113006 (1999).

[25] ATLAS Collaboration, JINST **3**, S08003 (2008).

[26] ATLAS Collaboration, arXiv:0901.0512 [hep-ex].

[27] ATLAS Collaboration, JHEP **1012** , 060 (2010) .

[28] M. Cacciari, G. P. Salam and G. Soyez, JHEP **0804**, 063 (2008).

[29] ATLAS Collaboration, Nucl. Instrum. Meth. A **621**, 134 (2010).

[30] ATLAS Collaboration, ATLAS-CONF-2011-032 (2011).

[31] ATLAS Collaboration, Eur.Phys.J. C**71**, 1577 (2011).

[32] CDF Collaboration, Phys. Rev. D**83**, 111101, (2011).

[33] D0 Collaboration, arXiv:1105.0320 [hep-ex].

[34] ATLAS Collaboration, ATLAS-CONF-2010-099 (2010).

[35] K. Nakamura et al. (Particle Data Group), J. Phys. G **37**, 075021 (2010).

[36] CDF and D0 Collaborations, arXiv:1007.3178 [hep-ex].

[37] S. Frixione, P. Nason and G. Ridolfi, JHEP **0709**, 126 (2007).

[38] B. P. Kersevan and E. Richter-Was, arXiv:hep-ph/0405247.

[39] G. Cowan, K. Cranmer, E. Gross and O. Vitells, Eur. Phys. J. C **71**, 1554 (2011).

[40] A. L. Read, J. Phys. G **28** 2693 (2002) .